

# Electrochemical Determination of Ascorbic Acid Based on Hydrothermal Synthesized ZnO Nanoparticles

*Hang Zhu and Guifen Xu*

Putian Univeristy, Dong Zhen West Road No. 450, Putian City, Fujian Province, 351100, P.R.China;  
E-mail: [journeysky@163.com](mailto:journeysky@163.com)

*Received: 22 February 2017 / Accepted: 22 March 2017 / Published: 12 April 2017*

---

In this work, ZnO nanoparticles (NPs) were prepared through an easy one-pot hydrothermal method. After synthesis, the obtained ZnO NPs were successfully adopted for surface modification of a glassy carbon electrode (GCE). The GCE modified with ZnO NPs was utilized to detect ascorbic acid (AA) in a sensitive and selective way. The biosensor revealed a linear correlation with AA concentration in the range of 1-800  $\mu\text{M}$ , with a limit of detection of 0.312  $\mu\text{M}$  (S/N = 3). The presented AA sensor manifested outstanding stability and repeatability and an anti-interference nature.

---

**Keywords:** ZnO; Hydrothermal synthesis; Electrochemical; Ascorbic acid; Sensor

## 1. INTRODUCTION

Ascorbic acid (AA) is a critical vitamin dispersed throughout the diet of both humans and animals. In plant cells, it exists in its free form, and at the same time, it is usually bound to proteins as ascorbigen. In respect to animal organs, the highest concentrations of AA are located in the liver leukocytes, and mammalian brain. Ascorbic acid has been frequently adopted to prevent and treat influenza, mental diseases, sterility and cancer. Various analytical methods, for example, titrimetric techniques, fluorometric analysis [1], spectrometry [2-4], chemiluminescence [5, 6], and liquid chromatography [7, 8], as well as enzymatic approaches [9], have been identified as effective tools for the detection of ascorbic acid. Among these methods, titration is deemed as the simplest approach for the detection of ascorbic acid, for which potassium iodate or bromate and dichlorophenol indophenol (DCPIP) have been applied [10]. Nevertheless, the dominating demerit of this approach is that it lacks specificity. The most frequently adopted technique for the precise detection of ascorbic acid is HPLC, but this method demands long specimen preparation time and complicated analysis operation. Other

analysis techniques, for example, spectrophotometric, enzymatic and chemiluminescence methods, fail to be applied frequently as a consequence of their analysis time and ascorbic acid degeneration.

In recent years, the development of chemical sensors to detect ascorbic acid electrochemically has aroused much attention. The electrochemical oxidization of ascorbic acid can be realized at many traditional electrodes that have been adopted for the detection of ascorbic acid [11, 12]. Ascorbic acid gives rise to a redox couple that is irreversible, forming dehydroascorbic acid. The electrocatalytic oxidation of ascorbic acid merely reveals an anodic oxidation peak. Through the single-directional reaction, an electroinactive product is formed, namely, 2,3-diketogulonic acid, which is formed when dehydro-L-ascorbic acid opens its lactone ring [13]. In the pH range of 2 to 4.5, ascorbic acid oxidation interchanges two protons in comparison with merely one when the pH range is 4.5 to 8. When the pH is higher than 8, two protons appear in the oxidized product. It has been shown that the ascorbate anion, namely, the intermediate, undergoes electrochemical oxidation to diketolactone, and then, it is dehydrated to dehydroascorbic acid, which further oxidizes to an ene-diol at higher potentials [14]. When the pH is above 8, the identification of the oxidation products is barely possible on account of the instabilities of ascorbic and dehydro-L-ascorbic acids in the basic solution [14]. The detection of ascorbic acid at clean electrodes is adversely affected by the excessively high potential and electrode fouling from its products after oxidation. In addition, biological molecules, such as dopamine, are likely to experience oxidation within a parallel potential window. As a result, electrode surface modification has been commonly used to improve the electrochemical nature of the detection of ascorbic acid.

Zinc oxide is a transition metal oxide that has been widely researched in electrochemistry. Research has shown that the addition of ZnO nanoparticles to graphene sheets has the capacity to improve the electrocatalytic performance of the complex material. In addition, Nayak et al. [15] illustrated an electrochemical dopamine sensor with excellent performance on the strength of the ZnO/graphene nanocomposite. Jiang and his coworkers [16] demonstrated a nanocomposite made by graphene and ZnO for the supersensitive electrochemical detection of paracetamol and acetophenetidin.

Consequently, this work illustrates the formation of one AA electrochemical biosensor on the basis of one-pot synthesized ZnO nanorods. The characterization of the synthesized ZnO was performed by scanning electron microscopy (SEM) and X-ray diffraction (XRD). The formed biosensor was adopted to realize AA detection through cyclic voltammetry (CV) and potentiostatic approaches. In comparison with a clean GCE, the results showed that the GCE modified with ZnO possessed a much higher current response and a lower oxidation potential.

## 2. EXPERIMENTS

Sigma-Aldrich was the provider of zinc nitrate hexahydrate ( $\text{Zn}(\text{NO}_3)_2 \cdot 6\text{H}_2\text{O}$ ), uric acid (UA), glucose, 3-hydroxytyramine hydrochloride (DA), ascorbic acid (AA),  $\text{H}_2\text{O}_2$  and acetylcholine (Ach). Commercial ZnO NPs were purchased from Xianfeng Nano Tech Co. Ltd. All other chemicals adopted in this process were of analytical grade and were used without any further purification. The preparation

of the phosphate buffer solution (PBS) was accomplished through mixing 0.1 M  $\text{KH}_2\text{PO}_4$  and  $\text{K}_2\text{HPO}_4$  solutions to a suitable pH. Milli-Q water (18.2 M $\Omega$  cm) was applied in the entire process.

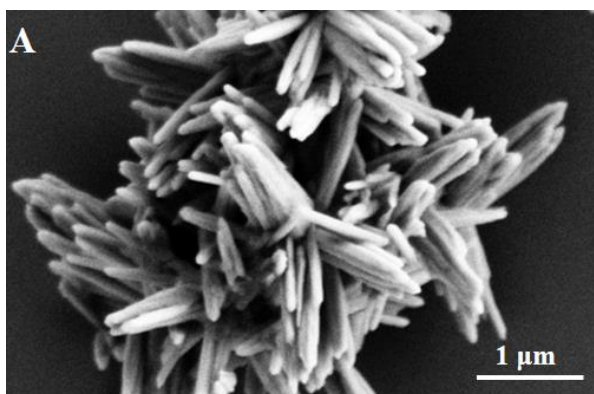
For the synthesis of ZnO, 10 mL of  $\text{Zn}(\text{NO}_3)_2 \cdot 6\text{H}_2\text{O}$  (50 mM) was added to a GO dispersion slowly with agitation. After the solution was sonication for one hour, 2 mL of hydrazine solution (5 wt%) was added as a blending agent. The gray slurry was stirred for 60 min and then was transferred to a 30-mL Teflon-lined non-rust steel autoclave and warmed up at a temperature of 120 °C for 2 h. The acquired specimens underwent centrifugation and exsiccation within a stove at 70 °C to give rise to ZnO NPs.

X-ray diffraction patterns were obtained in the  $2\theta$  range of 5°-90° through XRD using Cu  $K\alpha$  radiation (D8-Advanced, Bruker, Germany). Using a scanning electron microscope (SEM, S-4700, Hitachi High Technologies Corporation, Japan), the surface morphologies of specimens were studied.

For the electrochemical examinations, a GCE was polished with an alumina-water slurry and then was rinsed with water. For the modification of the electrode surface, 8  $\mu\text{L}$  of catalyst dispersion (0.5 mg/mL) was put onto the superficial layer of GCE and desiccated at room temperature. The conduction of the electrochemical measurements was accomplished on a CH Instruments 660A electrochemical workstation (CHI-660 A, CH Instruments, Texas, USA) with the adoption of a three-electrode setup. The counter electrode and reference electrode were platinum and Ag/AgCl (3 M KCl), respectively. CV was implemented in 0.1 M PBS within a scan range of 0.2 to 0.6 V at a scan rate of 50 mV/s. Amperometric response measurements were performed in 0.1 M PBS with fixed potential of 0.36 V under continuous stirring.

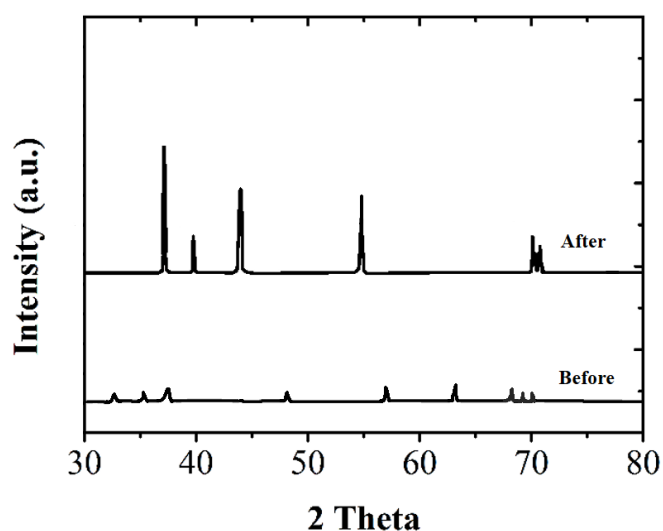
### 3. RESULTS AND DISCUSSION

Figure 1 illustrates an SEM image for the one-pot synthesized ZnO NPs. The ZnO NPs reveal a rod-like structure, with a mean length of 1.3  $\mu\text{m}$ . A further interesting observation is that each petal consists of some short, non-smooth and unformed nanorods. The ends of these rods attach to each other and form the tip-like petal. These nanostructured ZnO NPs are expected have large surface areas that could give rise to a high number of electrocatalytic sites for the reaction of molecules.



**Figure 1.** SEM image of the one-pot synthesized ZnO NPs.

Figure 2 shows the XRD patterns acquired for the ZnO NPs. The diffraction peaks of the ZnO NPs show up at  $31.4^\circ$ ,  $34.2^\circ$ ,  $35.7^\circ$ ,  $47.4^\circ$ ,  $56.2^\circ$ ,  $62.5^\circ$  and  $67.4^\circ$  and are indexed to hexagonal wurtzite ZnO (JCPDS Card 36-1451). In addition, the diffraction peak of GO at  $11.2^\circ$  vanishes together with the emergence of one novel wide peak at  $26.4^\circ$ , the (002) reflection, revealing that GO underwent reduction by the hydrothermal treatment. At the same time, all peaks appeared to shift to lower  $2\theta$  due to the improvement and higher density of the ZnO crystals when the calcination was finished. It can be concluded that the XRD pattern of the prepared specimen corresponds to the typical diffraction pattern of the hexagonal phase of ZnO, indicative of a wurtzite structure. Moreover, in comparison with other ZnO peaks, the intensity of the (001) reflection was higher, indicating the existence of a preferred orientation for the ZnO nanorods along the [001] orientation (vertical to the surface of the substrate), which is probably related to the preferential growth along the  $c$ -axis of the ZnO flowers [17].



**Figure 2.** XRD pattern of (A) as-prepared ZnO NPs as well as (B) annealed ZnO NPs.

Cyclic voltammograms (CVs) of ferricyanide are effective and convenient tools to monitor the surface status and barrier of the modified electrode, since the electron transfer between species in solution and the electrode must occur by tunneling either through the barrier or through the defects in the barrier. Well-defined oxidation and reduction peaks due to the  $\text{Fe}^{3+}/\text{Fe}^{2+}$  redox couple were observed in our experiment. It can be seen that the peak current at ZnO/GCE increased compared with the bare GCE because of an increase in the electroactive surface area of ZnO/GCE, which may be due to the ZnO layer formed on the surface of the electrode [18, 19]. The analysis of the electrochemical performance of 1 mM AA was separately realized through cyclic voltammetry at a clean GCE, commercial ZnO and the electrode modified with the prepared ZnO NPs (Figure 3). It can be seen in Figure 3 that there is no clear peak on the GCE modified with ZnO NPs when no AA is present. However, evident oxidization peaks of AA were seen on the clean GCE, GCE modified with ZnO NPs and commercial ZnO with current responses of 0.0107, 0.1154 and 0.0466 mA, respectively. In

addition, the oxidation potentials of AA on the clean GCE, GCE modified with ZnO NPs and commercial ZnO was 0.47, 0.36, and 0.44 V, respectively. As a consequence, the rise in the peak current together with the decline of the peak potential of the GCE modified with ZnO NPs are indicative of its outstanding electrocatalytic activity with respect to AA detection in comparison with the clean GCE and the GCE modified with commercial ZnO.

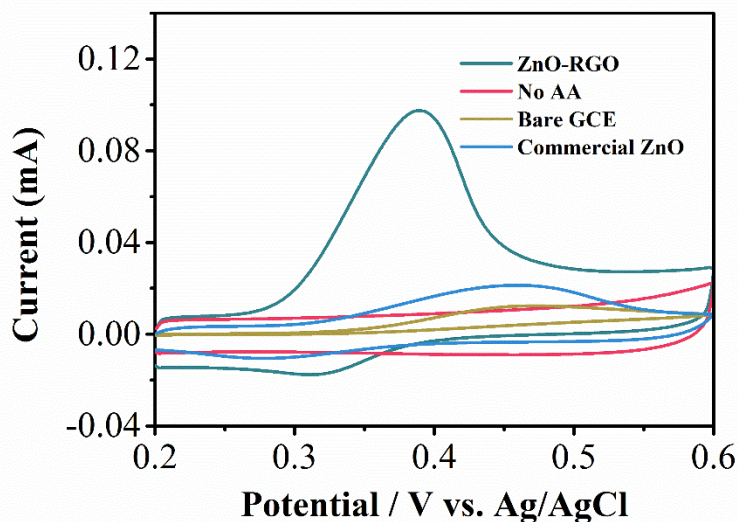


**Figure 3.** Cyclic voltammograms of a clean GCE, GCE modified with commercial ZnO and GCE modified with ZnO NPs in 0.1 M PBS without the addition of 1 mM AA. Scan rate: 50 mV/s.

The impact of the scan rate on the electrocatalytic oxidation of AA at the GCE modified with ZnO NPs was studied. The CVs utilizing the GCE modified with ZnO NPs with 1 mM AA were performed at scan rates of 20 to 260 mV/min. It can be seen in Figure 4A that the peak current increases with an increase in scan rate and that the oxidation potential shifts in the positive direction. This phenomenon was caused by the limitation of the kinetic energy of the reaction occurring between the AA and the active sites of the ZnO NPs, and this is consistent with previous studies [20, 21]. From Figure 4B, it can be seen that the peak current is linearly dependent on the square root of the scan rate, indicating that the reaction occurring on the superficial layer of the electrode is under the control of mass transfer. As a consequence, the following linear regression equation can be utilized:  $I_{pa} (\mu A) = 18.44v^{1/2} - 2.35$  ( $R^2 = 0.995$ ).

A linear regression can be acquired between the logarithm of the scan rate and the peak potential. It is represented in the following way:  $E_{pa} (V) = 0.09201 \log v + 0.23441$  ( $R^2 = 0.989$ ). On account of the linear equation, the number of electrons existing in the reaction can be ascertained via Laviron's equation [22, 23]:

$$E_p = E^{\circ'} + (2.303RT / \alpha nF) \log(RTk_0 / \alpha nF) + (2.303RT / \alpha nF) \log v$$

In the above equation,  $E^{\circ'}$ ,  $R$ , and  $\alpha$  represent the formal redox potential, the gas constant, and the electron transfer coefficient, respectively.  $F$  represents Faraday's constant, and  $k_0$  represents the reaction's standard heterogeneous rate constant. Since the slope of  $E_p$  versus  $\log v$  was determined to

be 0.09201, the  $\alpha n$  value can be figured out easily, namely, 0.5509. As a result,  $\alpha$  can be calculated in the following way:

$$E_{p/2} - E_p = 1.875(RT/\alpha F)$$

The value of  $\alpha$  was determined to be 0.7469. As a consequence, the overall number of electrons in the oxidation of uric acid is 2, which is consistent with earlier reports [20, 24, 25].

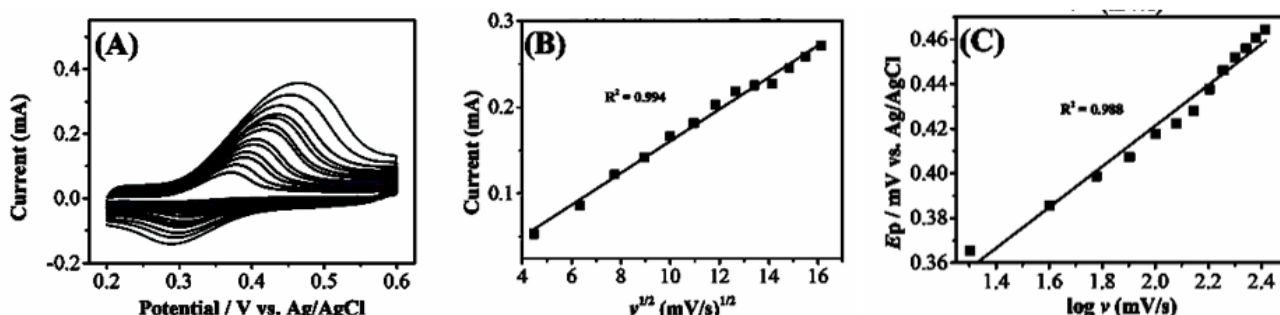


**Figure 4.** (A) Cyclic voltammograms recorded by the GCE modified with ZnO NPs at scan rates of 20–260 mV/s in 0.1 M PBS with 1 mM AA. (B) Plot of the peak current vs. the square root of the scan rate. (C) Plot of the peak potential vs. the logarithm of the scan rate.

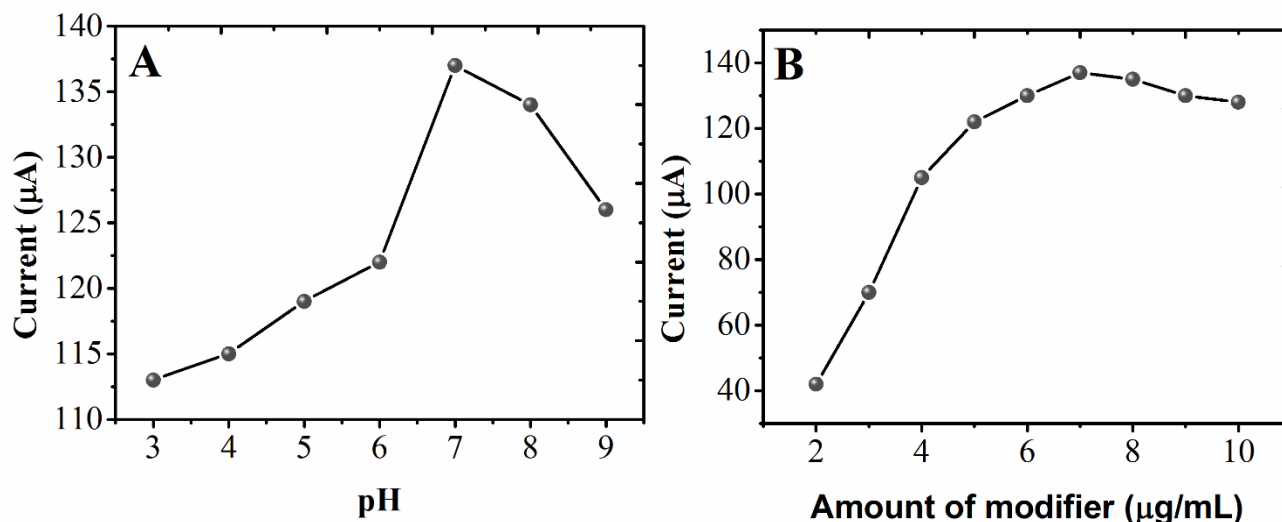


**Figure 5.** Plot of  $I_{pa}$  versus (A) pH of PBS and (B) quantity of added modifier for AA detection.

The effect of pH on the electrochemical detection of AA was studied as well. It can be found in Figure 5A that with a rise of pH from 3 to 7, the peak current also rises. The largest value was acquired when the pH was 7 (126.6  $\mu\text{A}$ ). With a further increase of the pH, there was a decline in peak current. As a result, pH 6 was utilized in the rest of the experiments.

Then, the influence of the amount of added modifier on the AA anodic peak current was analyzed. Figure 5B demonstrates that there was an evident increase in the peak current with a rise of the amount of added modifier from 2 to 7  $\mu\text{L}$ . When the amount of added modifier raised further, a

moderate decline in the current response was observed. This is likely caused by a longer electron transfer time for AA through the ZnO layer that has relatively high thickness.

Figure 6 shows the characteristic amperometric response under the successive addition of AA at the GCE modified with ZnO NPs. The GCE modified with ZnO NPs was found to have stable current within 7 s, indicative of the rapid response of the proposed sensor with respect to AA. Within the range of 1-800  $\mu\text{M}$ , a linear relationship between the AA concentration and the current response was seen. The linear regression equation is represented in the following way:  $I (\mu\text{A}) = 0.11561 C(\mu\text{M}) + 17.9307$  ( $R^2 = 0.998$ ). Through calculation, the limit of detection was found to be 0.27  $\mu\text{M}$  ( $S/N = 3$ ). Comparative research (as shown in Table 1) reveals that the sensor in this work could be adopted for the sensitive detection of AA.

**Table 1.** Comparison of diverse electrochemical sensors for detecting AA.

Electrode	Method	Linear range ( $\mu\text{M}$ )	Detection limit ( $\mu\text{M}$ )	Reference
Reduced graphene oxide/GCE	DPV	500—2000	150	[26]
Reduced graphene oxide/Au	DPV	240—1500	51	[27]
Pristine graphene	DPV	9—2314	0.9	[28]
Hemin-graphene oxide	DPV	3—100	0.3	[29]
Spherical MOF-5	DPV	0.7—11500	0.24	[30]
Au@Pd-reduced graphene oxide	DPV	1—800	0.28	[31]
ZnO NPs/GCE	I-T	1—800	0.27	This work

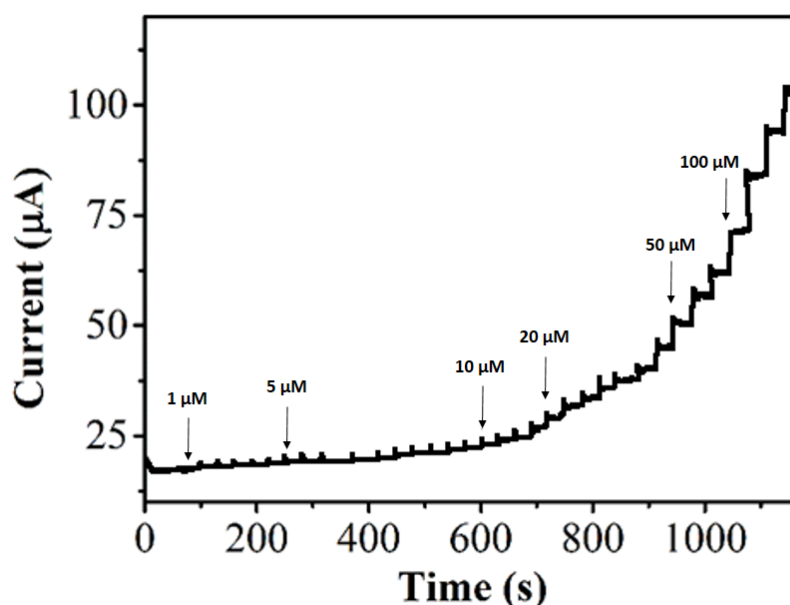


**Figure 6.** Amperometric response of the GCE modified with ZnO NPs under successive additions of AA in PBS (performed at 0.36 V).

With the purpose of analyzing the selective property of the sensor developed in this work, the effect of several physiological distractors were investigated. Figure 7 shows the characteristic amperometric response of the GCE modified with ZnO NPs with AA and some potential interference species, namely, DA, UA, glucose, H<sub>2</sub>O<sub>2</sub> and Ach. When 5 mM UA, DA, glucose, H<sub>2</sub>O<sub>2</sub> and Ach were added, no evident variation in the current response was observed, signifying the high selectivity of the fabricated sensor with respect to the detection of AA even when there was a 10-fold excess of general distraction substances.

The repeatability of the fabricated AA sensor was examined through detecting 0.5 mM AA with the adoption of six GCEs modified with ZnO NPs. The relative standard deviation (RSD) of the current responses was acceptable, namely, 2.4%. A steadiness test of the fabricated AA sensor was conducted with a constant I-T test for 10,000 s with 50  $\mu$ M AA. The experiment revealed that there was a 5% decline in current response of the fabricated AA sensor. The electrode response was very stable and showed excellent anti-fouling properties against the oxidation products. With the purpose of determining the storage steadiness for a long run, the GCE modified with ZnO NPs was tested after storing in an icebox for 14 days. The GCE modified with ZnO NPs showed a current response that maintained over 93% of the previous activity. Owing to this, the fabricated AA sensor possesses good steadiness and repeatability.

Through the measurement of AA concentrations in specimens of human urine and blood serum, the actual performance of the fabricated sensor was investigated. First, all specimens were diluted 100-fold with 0.1 M PBS. After this, in order to accurately determine the AA concentration, a standard addition approach was adopted. It can be seen in Table 2 that the recovery percentages of the four tests were within 98.37–103.15%. Consequently, the proposed AA sensor can be adopted to determine AA concentrations in practice. In addition, the AA concentrations in human serum specimens were evaluated. As revealed in Table 3, the recovery percentages of four tests were within 96.01–103.04%.

**Table 2.** Detection of AA in human urine and serum using the GCE modified with ZnO NPs.

Sample	Content ( $\mu$ M)	Added ( $\mu$ M)	Found ( $\mu$ M)	Recovery (%)
Urine 1	1.51	2.00	3.59	101.17
Urine 2	6.17	2.00	8.21	99.54
Serum 1	1.37	2.00	3.41	103.04
Serum 2	6.54	2.00	8.55	97.89

**Table 3.** Detection of AA in previous human serum.

Sample	Content ( $\mu$ M)	Added ( $\mu$ M)	Found ( $\mu$ M)	Recovery (%)
Urine 1	98.13	20.00	119.35	101.55
Urine 2	103.4	20.00	122.70	98.61

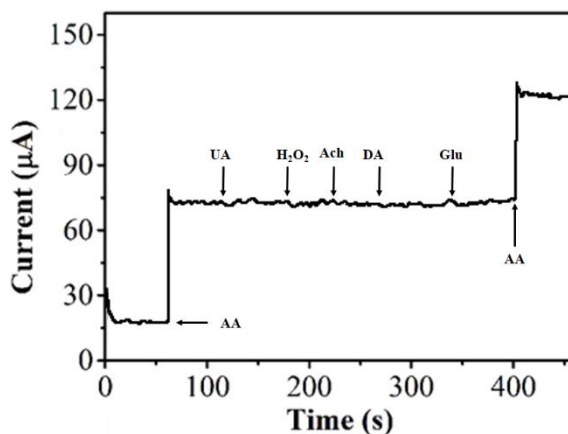


**Figure 7.** Amperometric current response of the GCE modified with ZnO NPs upon addition of 0.5 mM AA, 5 mM UA, 5 mM DA, glucose, H<sub>2</sub>O<sub>2</sub> and Ach at a working potential of 0.36 V.

#### 4. CONCLUSIONS

New ZnO NPs were fabricated using a one-pot hydrothermal approach. The GCE modified with ZnO NPs was adopted for the selective detection of AA. The AA sensor presented in this work revealed a broad detection scope with rapid response and relatively low detection limit. In addition, the sensor manifested an outstanding anti-interference nature and steadiness.

#### References

1. A. Lopez-Anaya and M. Mayersohn, *Clin. Chem.*, 33 (1987) 1874.
2. A. Jain, A. Chaurasia and K. Verma, *Talanta*, 42 (1995) 779.
3. S. Quan and W. Bei, *J. Anal. At. Spectrom.*, 10 (1995) 791.
4. M. Yebra, R. Cespon and A. Moreno-Cid, *Anal. Chim. Acta.*, 448 (2001) 157.
5. I. Agater and R. Jewsbury, *Anal. Chim. Acta.*, 356 (1997) 289.
6. Z. Zhang and W. Qin, *Talanta*, 43 (1996) 119.
7. E. Oliveira and D. Watson, *J. Chromatogr. B.*, 764 (2001) 3.
8. M. Kall and C. Andersen, *J. Chromatogr. B.*, 730 (1999) 101.
9. W. Lee, S. Roberts and R. Labbe, *Clinical chemistry*, 43 (1997) 154.
10. G. Deshmukh and M. Bapat, *Fresenius' Zeitschrift für Analytische Chemie*, 145 (1955) 254.
11. X. Zuo, H. Zhang and N. Li, *Sens. Actuators, B.*, 161 (2012) 1074.
12. J. Zen, D. Tsai, A.S. Kumar and V. Dharuman, *Electrochem. Commun.*, 2 (2000) 782.
13. J. Ruiz, A. Aldaz and M. Dominguez, *Can. J. Chem.*, 55 (1977) 2799.
14. M. Rueda, A. Aldaz and F. Sanchez-Burgos, *Electrochim. Acta*, 23 (1978) 419.
15. P. Nayak, P. Santhosh and S. Ramaprabhu, *Graphene*, 1 (2013) 25.
16. L. Jiang, S. Gu, Y. Ding, F. Jiang and Z. Zhang, *Nanoscale*, 6 (2014) 207.
17. J. Liu, X. Huang, Y. Li, J. Duan and H. Ai, *Mater. Chem. Phys.*, 98 (2006) 523.
18. E. Molaakbari, A. Mostafavi, H. Beitollahi and R. Alizadeh, *The Analyst*, 139 (2014) 4356.
19. M. Marie, S. Mandal and O. Manasreh, *Sensors*, 15 (2015) 18714.
20. D. Oukil, L. Benhaddad, R. Aitout, L. Makhloufi, F. Pillier and B. Saidani, *Sens. Actuators, B.*, 204 (2014) 203.

21. Y. Wei, M. Li, S. Jiao, Q. Huang, G. Wang and B. Fang, *Electrochim. Acta*, 52 (2006) 766.
22. E. Laviron, *J. Electroanal. Chem.*, 52 (1974) 355.
23. E. Laviron, *J. Electroanal. Chem.*, 101 (1979) 19.
24. X. Cao, Y. Xu, L. Luo, Y. Ding and Y. Zhang, *J. Solid State Electrochem.*, 14 (2010) 829.
25. H. Manjunatha, D.H. Nagaraju, G. Suresh and T. Venkatesha, *Electroanalysis*, 21 (2009) 2198.
26. L. Yang, D. Liu, J. Huang and T. You, *Sens. Actuators, B.*, 193 (2014) 166.
27. C. Wang, J. Du, H. Wang, C.e. Zou, F. Jiang, P. Yang and Y. Du, *Sens. Actuators, B.*, 204 (2014) 302.
28. S. Qi, B. Zhao, H. Tang and X. Jiang, *Electrochim. Acta*, 161 (2015) 395.
29. H. Zou, B. Li, H. Luo and N. Li, *Sens. Actuators, B.*, 207, Part A (2015) 535.
30. Y. Song, C. Gong, D. Su, Y. Shen, Y. Song and L. Wang, *Analytical Methods*, 8 (2016) 2290.
31. J. Jiang and X. Du, *Nanoscale*, 6 (2014) 11303.

© 2017 The Authors. Published by ESG ([www.electrochemsci.org](http://www.electrochemsci.org)). This article is an open access article distributed under the terms and conditions of the Creative Commons Attribution license (<http://creativecommons.org/licenses/by/4.0/>).